Hybrid multiple diffraction in semipolar $(01\bar{1}2)$ oriented wurtzite materials: ZnMgO/ZnO as an illustration

Esther de Prado,[a]* M.Carmen Martínez-Tomás,[a] Christiane Deparis,[b] Vicente Muñoz-Sanjosé[a] and Jesús Zúñiga-Pérez[b]

[a]*Departamento de Física Aplicada y Electromagnetismo, Universidad de Valencia, Dr. Moliner* 50, 46100 *Burjassot Spain, and* [b]*UCA, CRHEA-CNRS, Rue Bernard Gregory,* 06560 *Valbonne France. E-mail: esther.prado@uv.es*

Abstract

X-ray diffraction has been widely used to characterize the structural properties (strain and structural quality) of semiconductors heterostructures. In this work, we employ hybrid multiple diffraction to analyze r-oriented $Zn_{1-x}Mg_xO$ layers grown by molecular beam epitaxy on ZnO substrates. In such a low-symmetry material system, additional features appear in symmetric-reflections scans, which we describe as arising from hybrid multiple diffraction. We first introduce the Bragg conditions necessary for these high-order processes to occur and apply them to explain all the observed satellite reflections, identify the planes that contribute and compute *a priori* the angles at which they are observed. Furthermore, thanks to this hybrid multiple-diffraction technique we have been able to determine the layer lattice parameters in an easy and accurate way by using one single measurement in standard symmetric conditions. The achieved precision is, at least, as high as that obtained from the combination of symmetric and asymmetric reciprocal space map measurements.

1. Introduction

X-ray diffraction is a very useful characterization tool since it provides information on the crystalline quality of materials and their strain in a non-destructive manner. Beyond the routine measurements such as rocking curves, $2\theta - \omega$ scans, reciprocal space maps (RSM)..., which employ a two-beam geometry, the analysis of multiple diffraction (MD) processes could provide an alternative method for the structural characterization of samples. MD takes place when more than one reciprocal point lies in the Ewald sphere so that diffraction involving two (or more) sets of planes ends up matching the direction of another family of diffracting planes. Experimentally, since it is not possible to discriminate the contributions to diffraction between two-beam diffraction and MD, this phenomenon is generally studied for forbidden or very weak reflections, in which changes in intensity may be more easily observed (Chuanzheng *et al.*, 2000). It was first reported by Renninger in 1937 (Renninger, 1937) and used for the (222) reflection of diamond, obtaining accurately its lattice parameters (Renninger, 1955). With the same aim and also for the analysis of surface perfection it was later on employed by Cole *et al.* (Cole *et al.*, 1962), for germanium, and by Post and coworkers, (Post, 1975; Hom *et al.*, 1975) for diamond, silicon and germanium. More recently, MD has been used for the analysis of GaN and ZnO wurtzite materials by several authors, including Bläsing *et al.* (Biäsing & Krost, 2004), Martínez-Tomás *et al.* (Martínez-Tomás *et al.*, 2012; Martínez-Tomás *et al.*, 2013*b*) and Grundmann *et al.* (Grundmann *et al.*, 2014). From a general perspective, MD provides information on crystal symmetry, crystal quality and defects (Chang, 1982; Morelhão & Cardoso, 1996).

In heteroepitaxial systems, so-called Hybrid Multiple Diffraction (HMD) can happen, which is a particular and poorly studied kind of multiple diffraction: in this case both layer and substrate are involved in the generation of MD, giving rise to

a hybrid reciprocal space much more complex than just a superposition of the bare substrate/layer reciprocal spaces. One of the first studies in this frame was performed by Isherwood *et al.* (Isherwood *et al.*, 1981), who investigated cubic $Ga_{1-x}Al_xAs$ epitaxially grown on (001) GaAs substrates. Later, it was studied by Morelhão *et al.* (Morelhão & Cardoso, 1991; Morelhão *et al.*, 1991; Morelhão & Cardoso, 1993; Morelhão *et al.*, 2003; Morelhão & Domagala, 2007) and Domagala and coworkers (Domagała *et al.*, 2016) for different cubic and, ultimately, for wurtzite *c*-oriented materials.

The ternary alloy ZnMgO has been revealed as an interesting material in view of its applications on a variety of photonic and electronic devices of technological relevance (Ohtomo *et al.*, 1998). So-called semipolar materials, with growth surfaces inclined to (00.1) polar plane, are expected to have reduced internal electrical fields and high intrinsic exciton lifetime. However these orientations, as that of *r*-wurtzite ZnMgO, present intrinsic difficulties in their structural characterization related to the low symmetry of this system. The valuable information one can obtain by using HDM technique of characterization, which to the best of our knowledge has never been used to analyze wurtzite semipolar orientations, and the great technological interest of the ZnMgO/ZnO system has been the reason to develop this study.

To illustrate the power of this X-ray diffraction approach and the valuable information one can obtain for wurtzite materials thanks to it, in this work ZnMgO layers grown on *r*-oriented ZnO substrates have been selected. Indeed, ZnO and GaN share many physical properties and in particular their wurtzite crystalline structure (Zúñiga-Pérez *et al.*, 2016), with ZnMgO playing the role of AlGaN in the context of bandgap engineering. However, contrary to AlGaN, for which both a and c-lattice parameters decrease with Al composition (Angerer *et al.*, 1997), ZnMgO displays a peculiar behavior, with a increasing with Mg content and c decreasing with it (von Wenck-

stern *et al.*, 2012). As will be shown later, this peculiar behavior of the ZnMgO lattice parameters (Grundmann & Zúñiga-Pérez, 2015) will result in some specific features. The article is organized as follows: after a brief description of the measured samples, a complete analysis of the hybrid reflections based in the combined substrate-layer reciprocal space will be made, which will provide the expected angular positions of hybrid peaks; these calculations will be subsequently employed to associate the proper indexes to the hybrid reflections and identify the planes involved in the MD process. Finally, HMD will be exploited to easily determine the c and a lattice parameters based on measurement of symmetric scans. The accuracy of these lattice parameters will be compared to that obtained by measuring symmetric and asymmetric reciprocal space maps, as commonly done in the literature.

2. Experimental Details.

$Zn_{1-x}Mg_xO$ layers were epitaxially grown on a buffer layer of ZnO grown itself homoepitaxially on commercial semipolar (01.2) ZnO substrates purchased from Crystec. The dot represents the third redundant index of the Miller-Bravais notation. The Riber Epineat MBE system is equipped with effusion cells for elemental Zn and Mg, and a radiofrequency plasma cell for atomic oxygen (a radiofrequency power of 420 W was used). The samples were grown at a growth temperature of around 400°C. Before introducing the ZnO substrates into the reactor they were annealed at high temperature (1100°C) in an oxygen atmosphere. The Mg content was determined by microanalysis in a scanning electron microscope (SEM) equipped for energy-dispersive X-ray spectroscopy and was confirmed by optical spectroscopy measurements, while the thickness of the samples was determined directly by measuring it in cross-section. HRXRD beam measurements were performed in a Panalytical X-Pert MRD diffractometer with Cu tube. Parallel Kα_1 irradiation was ensured by a parabolic mirror

and a 4-bounce hybrid monochromator situated in the incident beam. A three-bounce (220) Ge analyzer crystal was placed in the diffracted beam. The X-ray beam divergences were 0.005° in the incidence plane and 2° in the axial direction.

3. Theory

3.1. Multiple diffraction

The analytical calculation of MD peaks here presented follows the treatment of Morelhão *et al.* (Morelhão & Domagala, 2007), which has been adapted to *r*-oriented hexagonal crystals. As already introduced, MD arises when more than one lattice point lie on the Ewald sphere for an incident beam $\vec{k}_0$. That is, when for a given incident beam there are more than one set of planes that fulfill simultaneously the Bragg condition. When two sets of planes are involved (three beam diffraction), we will refer to them as primary and secondary, with diffraction vectors $\vec{P}$ and $\vec{S}$ respectively. In the current treatment the primary reflection will involve planes parallel to the surface of the sample (symmetric reflection), while the secondary reflection is related to planes tilted with respect to the surface (asymmetric reflections).

The Bragg conditions for the primary and secondary reflections are, respectively:

$$\vec{k}_0 \cdot \vec{P} = -\vec{P} \cdot \vec{P}/2 \tag{1}$$

$$\vec{k}_0 \cdot \vec{S} = -\vec{S} \cdot \vec{S}/2 \tag{2}$$

Since the secondary beam is diffracted by a third set of planes (cooperative planes with diffraction vector $\vec{C}$) towards the outgoing primary direction, we have

$$\vec{P} = \vec{S} + \vec{C}$$

and the Bragg condition for the cooperative reflection is written

$$\vec{k}_0 \cdot \vec{C} = -\vec{C} \cdot \vec{C}/2 - \vec{C} \cdot \vec{S} \tag{3}$$

Figure 1 shows two particular cases of diffraction in which the incident beam, primary, secondary and cooperative diffraction vectors are coplanar. The three-beam X-Ray diffraction condition can be fulfilled by rotating the sample around the primary diffraction vector $\vec{P}$ of the reflection whose intensity is monitored, generally a symmetric one. The secondary and cooperative reflections will be excited only at some specific azimuthal angles φ_0 of the incident direction, as in Renninger scans. This angle can be calculated by entering $\vec{k}_0$ and $\vec{S}$ in the Bragg condition of the secondary planes, eqn. 2

$$\vec{k}_0 = -\left|\vec{k}_0\right| \left[\cos\omega_0 \cos\varphi_0 \vec{u}_x + \cos\omega_0 \sin\varphi_0 \vec{u}_y + \sin\omega_0 \vec{u}_z\right] \tag{4}$$

$$\vec{S} = \left|\vec{S}\right| \left[\sin\gamma \cos\alpha\, \vec{u}_x + \sin\gamma \sin\alpha\, \vec{u}_y + \cos\gamma \vec{u}_z\right] \tag{5}$$

$$\cos\beta = \frac{\lambda \left|\vec{S}\right| /2 - \sin\omega_0 \cos\gamma}{\cos\omega_0 \sin\gamma} \tag{6}$$

$$\varphi_0 = \alpha \pm \beta \tag{7}$$

where λ is the wavelength of the X-ray beam, ω_0 the incidence angle for the primary reflection, γ is the angle between the primary and secondary diffraction vectors and α is the angle between the secondary diffraction vector and a reference direction.

The aforementioned φ_0 must be computed with respect to the same reference direction. Unitary vectors are defined by the selected orthogonal system described in the next paragraph.

Our choice of orthogonal axes is shown in Figure 2, where the X axis matches the $[0\bar{1}.1]$ direction, the Y axis matches the $[2\bar{1}.0]$ direction and the Z axis is perpendicular to the (01.2) plane. The origin for the azimuthal angle has been chosen also in the X-axis. Then, the expected direction between the incidence and the reference direction in which MD can be observed is given by $\varphi_0 = \alpha \pm \beta$. When MD takes place in *c*-oriented wurtzite materials (Grundmann *et al.*, 2014), due to the actual crystal symmetry the distribution of MD peaks is periodic with a period of 60° (i.e. $\varphi_n = \varphi_0 + n\pi/3$ with integer n in equivalent reflections). In our case, due to the low symmetry of the *r*-wurtzite orientation, we find only a periodic repetition of 180°, $\varphi_n = \varphi_0 + n\pi$, as will be shown later.

3.2. Multiple diffraction in heterostructures

When heteroepitaxial structures are considered, the usual vision of the reciprocal space is a superposition of two reciprocal lattices, one from the substrate and another from the layer. In this situation, if MD occurs exclusively within the substrate, or exclusively within the layer, no extra features in reciprocal space are generated, since sums of diffraction vectors $\vec{S}$ and $\vec{C}$ always end up at a reciprocal-lattice point. HMD arises when the secondary and cooperative planes belong to different reciprocal lattices (either that of the substrate, S, or that of the layer, L, or viceversa):

$$\vec{P}_H = \vec{S}_L + \vec{C}_S \tag{8a}$$

$$\vec{P}_H = \vec{S}_S + \vec{C}_L \tag{8b}$$

In reciprocal space these conditions lead to a hybrid diffraction vector $\vec{P}_H$ that can differ in magnitude, direction or both with respect to the primary one $\vec{P}$, as can be seen in Figure **??**. In this figure we display a scheme of the reciprocal space for *c*-oriented and *r*-oriented systems.

Figure 3a) corresponds to a *c*-oriented system in which the epilayer is completely relaxed. It can be observed that the hybrid vectors near the symmetric reflection have different directions, but maintain a similar magnitude, exhibiting hybrid points at both sides of the out-of-plane axis. This case is equivalent to that treated by Morelhao *et al.* (Morelhão & Domagala, 2007) for cubic ZnSe/GaAs (001) structures.

In Figure 3b) a scheme of reciprocal space is depicted when fully strained or epitaxial layers are considered. In this case there is a negligible change in the direction of hybrid diffraction vector, and layer, substrate and hybrid peaks are nearly aligned along the out-of-plane axis. This is similar to the situation analyzed by Domagala *et al.* (Domagała *et al.*, 2016) with $Al_{0.14}Ga_{0.86}N$ epilayers grown on GaN (00.1) substrates.

Figure 3c) shows a scheme of the reciprocal space for *r*-oriented samples in the plane that contains the *c*-axis and for an epilayer considered to be fully strained. This is the situation analyzed in this work, for which the fully-strained conditioned was assessed by measuring RSM of asymmetric reflections (a more detailed discussion on the measurement of the lattice parameters for *r*-oriented heterostructures grown on ZnO substrates will be given elsewhere). For this orientation, and when considering the ZnMgO/ZnO material system, the most outstanding characteristic is that the layer points are located above/below the substrate points depending on their position with respect to the out-of-plane axis (*r*-axis). This is a consequence of the peculiar behavior of the ZnMgO lattice parameters (a and c) as a function of the Mg concentration, given that the signs of the change of lattice parameters with concentration show opposite signs (Ohtomo *et al.*, 1998).

As the interplanar distance for a hexagonal structure is:

$$\frac{1}{d_{hkl}^2} = \frac{4}{3}\frac{h^2 + k^2 + hk}{a^2} + \frac{l^2}{c^2}$$

Directions in which the contribution of a lattice parameter is higher, the following

condition is fulfilled $d_{hkl}(ZnO) < d_{hkl}(ZnMgO)$ and just the opposite for directions in which c parameter is the dominant factor, so there is a direction in which both interplanar distances are equal. Thus, in our system where ZnO is the substrate and $Zn_{1-x}Mg_xO$ the layer, for the plane that contents the c-axis (points contained in the reciprocal space $(0k.l)$ plane, depicted in Figure 3c), there is a direction near the "r-axis" that marks this change of signs and fulfills the condition

$$\frac{4}{3}k^2\left(\frac{1}{a_S^2}-\frac{1}{a_L^2}\right)=l^2\left(\frac{1}{c_L^2}-\frac{1}{c_S^2}\right) \tag{9}$$

where a_S , c_S and a_L , c_L are the lattice constants of substrate and layer, respectively. At either side of this "crossover-line", the influence of the c- or of the a-lattice parameter is most important and the reciprocal lattice point of the ZnMgO layer lie above or below those of the ZnO substrate, respectively. Hybrid points lie along the out-of-plane axis nearly aligned with the substrate and layer points. In addition, the absolute value of the hybrid diffraction vector changes considerably, as illustrated in Figure 3d), which shows the symmetric 01.2 RSM for one of our samples at $\varphi = 90°$. The map displays the layer (L), substrate (S) and hybrid (H) points.

3.3. Hybrid peak positions

In real space this change in magnitude of the hybrid diffraction vector $\vec{P}_H$ implies that the Bragg angle of the hybrid reflection does not coincide exactly with the Bragg angle of the symmetric reflection, neither of the layer nor of the substrate. That is, the final beam is not diffracted towards the outgoing primary direction (θ) but in a direction very close to it (θ_H). The Bragg angle of hybrid peaks (θ_H) can be calculated in the framework of the previous analysis by applying the Bragg law to the diffraction vector $\vec{P}_H$ obtained by eqns. 8

$$\frac{2}{|\vec{P}_H|}\sin\theta_H = n\lambda \tag{10}$$

The choice of eqn. 8a or 8b to determine $\vec{P}_H$ or, equivalently, the indexation of hybrid peaks, has to be done by comparing calculated and experimental values of the θ_H.

The incident azimuthal angle φ_0 at which MD is expected is given by eqn. 6. However, when HMD happens the incidence vector can follow a different path within the sample due to the different lattice constants of the substrate/layer so that incidence and exit vectors need not be contained within the same plane defined by the sample normal and either of them (see Figure 4). In this case there is an azimuthal angular difference of $180° + \Delta\varphi$ between the direct/reverse sense of the path. This difference can be calculated by applying eqn. 6 to both the direct/reverse path of a hybrid reflection with incident angle ω. If in the direct sense the secondary reflection takes place first on the substrate, consequently, in the reverse sense the reflection will be first in the layer and then in the substrate

$$\cos\beta = \frac{\lambda\left|\vec{S}_S\right|/2 - \sin\omega\cos\gamma_S}{\cos\omega\sin\gamma_S} \tag{11a}$$

$$\cos\beta' = \frac{\lambda\left|\vec{S}_L\right|/2 - \sin\omega\cos\gamma_L}{\cos\omega\sin\gamma_L} \tag{11b}$$

The azimuthal angular difference in the trajectory path will be given by $\Delta\varphi = \beta - \beta'$

.

This calculation method is easier than those used in other studies (Morelhão & Cardoso, 1996; Morelhão *et al.*, 2003; Morelhão & Domagala, 2007) where authors calculate the incidence conditions in a hybrid system by solving a two equations system.

4. Results and discussion

Occurrence of HMD in *r*-oriented ZnMgO/ZnO heterostructures has been analyzed in samples with three different Mg contents of $27 \pm 3\%$, $35 \pm 6\%$ and $43 \pm 5\%$, as determined by EDX and confirmed by optical measurements. These samples have different thicknesses and we will refer to them as S27, S35 and S43 respectively (see Table 1). Satellite peaks in $2\theta - \omega$ scans (Figure 5), besides those corresponding to the substrate and layer (as well as those associated to Pendellösung fringes for the two thinnest samples), were observed for all three samples. Two families of hybrid peaks observed at two different 2θ Bragg angles and for different φ positions could be identified. The one with lower Bragg angle appears with an approximated six-fold symmetry in φ, at $\sim 0^\circ$, $\pm 60^\circ$, $\pm 120^\circ$ and 180° with respect to the φ reference angle (the X axis); we will refer to them as P1-P6 peaks. The other family, at a higher 2θ angle, has a two-fold symmetry in φ and is found at $\pm 90^\circ$ (P7 and P8 peaks). Due to the low thickness of the layer in sample S35, the positions of these additional peaks were determined by simulation of the complete XRD pattern. These "additional" peaks depend clearly on the Mg content of the epilayer, as shown in Figure 5d), where it can be seen that the $2\theta_H$ values of hybrid peaks converge towards the position of the ZnO peak. This dependence of the $2\theta_H$ values on the Mg content is consistent with the HMD scheme described before, since for the limit case of 0% Mg both secondary and cooperative reflections belong to the substrate reciprocal space, so no extra features should be found.

To prove that these additional peaks are in fact a consequence of HMD, we have carried out the indexation of planes that are involved in their generation, we have calculated the expected theoretical Bragg and azimuthal angles at which they are expected, and we have confronted all these calculations to the experimental findings.

4.1. Indexation of participating planes and azimuthal positions

In order to determine the participating planes and the expected angles, all the kinematically allowed reflections (for the secondary and cooperative planes) were systematically investigated. Theoretical values of the Bragg ($2\theta_{theo}$) and azimuthal (φ_{theo}) angles at which HMD is expected were provided by eqn. 10 and 11, respectively, and the needed lattice constants were determined by RSM measurements. A slight orthorhombic distortion of the ZnMgO basal plane was observed for all the samples (de Prado *et al.*, Unpublised) and, thus, the values of the lattice parameters used in the calculations refer to mean values. Finally, the planes that match better the experimental angles were selected. Table 2 displays these planes and their characteristic angles.In all calculations the tilt and twist of the layer with respect to the substrate has been taken into account.

It has been found that, for a given azimuthal angle, different sets of planes contribute to the same hybrid peak: two at 0°, ±90° and 180° and three at ±60° and ±120°. That is, each hybrid peak is generated by two or three combinations of secondary-cooperative set of planes, as indicated in Table 2. It is outstanding that the total number of planes that are involved in the HMD peaks considered in this study is low. More precisely, 5 combinations of secondary and cooperative planes are found to explain the experimental hybrid peaks: $(\overline{1}1.5)_S + (10.\overline{3})_L$, $(10.5)_S + (\overline{1}1.\overline{1})_L$, $(0\overline{1}.3)_S + (02.\overline{1})_L$, $(00.4)_S + (01.\overline{2})_L$, $(00.2)_S + (01.0)_L$. The sets of planes that contribute to a hybrid peak in φ are the same as those that contribute in $\sim \varphi + 180°$. This is explained by the fact that the beam path is the same but in the reverse sense. The low number of observed HMD peaks is not surprising, given the low symmetry of the system and the expected reduced intensities of MD reflections in ternary compounds, as they are extremely sensitive to the content of the alloy (Biäsing & Krost, 2004; Grundmann *et al.*, 2014).

Figure 6*a*) shows the azimuthal positions at which HMD appears in sample S43 as a function of the wavelength and taking into account all the previous sets of planes. A two-fold symmetry around $\varphi = 0^\circ$ can be observed due to the mirror symmetry of the wurtzite *r*-plane across the plane containing the *c*-axis. Obviously in higher-symmetries configurations, such as *c*-wurtzite ZnO (Martínez-Tomás *et al.*, 2013*b*; Grundmann *et al.*, 2014; Martínez-Tomás *et al.*, 2013*a*), similar calculations give smaller azimuthal periodicities. In our case, due to the low symmetry of the *r*-oriented wurtzite structure, the whole interval 0° to 180° has to be considered. It can be seen that the predicted azimuthal angles at which HMD is expected using the $K\alpha_1$ wavelength are effectively 0°, ±60°, ±120° and 180° for P1-P6 peaks and at ±90° for peaks P7 and P8. Hybrid peaks are best observed in ω/φ maps.

Figures 6b) and 6c) show these maps for sample S43 at both, low and high hybrid Bragg angles respectively. Periodicity in φ of hybrid peaks is clearly seen, whereas the intensity associated to the substrate peak is observed whatever the azimuthal angle.

The calculated values for the azimuthal angles are given in Table 2. For a given peak, the azimuthal spread of the calculated contributions span an azimuthal range of 1.4° or less (see P5 for the S43 sample). This range falls within the FWHM of the experimental peaks. Another factor that can contribute to this spread is the orthorhombic distortion, which might not be homogenous for all the thickness. Most importantly, calculated and measured azimuthal values coincide for all peaks.

As introduced earlier in the article, when HMD takes place, the incidence and exit X-ray trajectories for a given combination of secondary and cooperative planes need not be at 180° azimuthally. These azimuthal deviations ($\Delta\varphi$) in the beam path can be calculated through eqns. 11a and 11b and are shown in Table 3. In all cases, the azimuthal deflection indicates a twist of the beam path towards the plane that contains the *c*-axis ($\varphi = 180^\circ$), as shown in Figure 4. Again, the agreement between

calculations and experiments is excellent. Similarly, for a given azimuthal angle it can be seen that the different combinations of planes give rise to slightly different $2\theta_H$ values but, once again, the agreement between theoretically calculated values and measured ones is excellent. The combination of all of them gives rise to wide peaks. This is illustrated for peaks P3 and P7 in figure 7*a* and 7*b* respectively. In these maps the FWHM in Bragg angle (abscissa axis) is clearly smaller than the FWHM in the phi angle (ordinate axis). This behavior matches the theory, since the spread of theoretical $2\theta_H$ values for a given peak is much smaller than the corresponding spread for the azimuthal values, typically 0.1° against 1.4°.

4.2. Lattice parameters calculation

Once that occurrence of HMD has been demonstrated and planes involved have been determined, next we will show how the lattice parameters can be obtained by measuring just one RSM on a symmetric reflection. Thus, both lattice parameters (a and c) can be obtained without the need of measurement on asymmetrical reflections. The method will be applied to $Zn_{1-x}Mg_xO$ layer grown on an r-oriented ZnO substrate but can be generalized to other orientations easily.

For this purpose it is enough to obtain a RSM of a symmetric reflection at an azimuthal angle at which a hybrid peak appears and in which substrate, layer and hybrid peaks are observed together. In our case, we have chosen the hybrid peak observed at $\varphi = 90^\circ$ generated by planes $(00.2)_S$ and $(01.0)_L$ due to its relative large intensity.

Once this map is obtained, the analysis of the out-plane coordinates q_z for the layer and hybrid peaks will give the layer lattice parameters. This coordinate, for the point corresponding to the layer $q_z(01.2)_L$, is related to the lattice constants of the layer (a_L, c_L) through (Cullity & Stock, 2001)

$$q_z(01.2)_L = 2\sqrt{\frac{1}{3a_L^2} + \frac{1}{3c_L^2}} \tag{12}$$

On the other hand, eqn. 8 gives the relation between the measured coordinates for the hybrid peak ($q_z(01.2)_H$) and the lattice constants of substrate (a_S, c_S) and layer

$$q_z(01.2)_H = q_z[(00.2)_S + (01.0)_L] = \frac{2}{c_S^2\sqrt{\frac{1}{3a_S^2} + \frac{1}{c_S^2}}} + \frac{2}{3a_L^2\sqrt{\frac{1}{3a_L^2} + \frac{1}{c_L^2}}} \tag{13}$$

As the lattice constants of the ZnO substrate are known, lattice constants of the layer can be obtained by solving the above system. Anisotropic strains can be detected if symmetric RSM points are obtained at other azimuthal angles where hybrid peaks appear, but will not be discussed here (de Prado *et al.*, Unpublised).

For the sake of comparison, Table 4 displays the calculated lattice constants for samples S27 and S43 using the typical combination of RSMs on symmetric and asymmetric reflections and those calculated from the experimental value of the hybrid Bragg angle and the procedure proposed here using high resolution HMD. As can be seen, by using the high-resolution HMD procedure described here both lattice parameters can be obtained with high accuracy (as large as that obtained by combining symmetric and asymmetric RSMs) and employing roughly half of the time.

5. Conclusions

HMD is a particular case of multiple X-Ray diffraction. In this work we report on the existence and interpretation of HMD in a low symmetry epilayer/substrate system as exemplified by the *r*-wurtzite crystallographic orientation. In order to obtain a complete understanding of this phenomenon we have analyzed the planes that contribute to the generation of hybrid peaks and calculated their angular positions (φ_H and $2\theta_H$).

For the particular case of *r*-oriented ZnMgO/ZnO heterostructures, two sets of hybrid reflections were found, the lower one with an approximate six-fold symmetry

and the higher one with a two-fold symmetry in the azimuthal angle. Interestingly, for these hybrid reflections the projection of the beam path on the sample surface is not a straight line, the out-coming beam being slightly deviated with respect to the incoming one towards the plane that contains the c-axis. In spite of the low symmetry of the r-wurtzite structure five sets of planes have been shown to contribute to the HMD. Calculated and experimental values of hybrid angles, azimuthal positions and deviations of the trajectory agree admirably well.

The analysis and angular precision achieved leads us to propose the use of HMD for the accurate measurement of lattice parameters. This method provides an easy way to shorten the measurement time without sacrifying accuracy.

In conclusion, instead of being avoided, hybrid reflections should be better explored since they provide a quick and nondestructive tool for a comprehensive characterization of semiconductor heterostructures.

This work was done under financial support from the Spanish Ministry of Economy and Competitiveness (MINECO) under project TEC2014 − 60173 and by the Generalitat Valenciana under the projects Prometeo II 2015/004 and ISIC/2012/008, as well as from the ANR through the project PLUG-AND-BOSE. E. de Prado thanks for the Grants No. BES-2012 − 058988 and No.EEBB-I-15 − 09749. The authors are grateful to the Central Support Service in Experimental Research (SCSIE), University of Valencia, Spain, for providing XRD facilities, and to O. Tottereau for support in EDX measurements.

References

Angerer, H., Brunner, D., Freudenberg, F., Ambacher, O. & Stutzmann, M. (1997). *Appl. Phys. Lett.* **1504**(71), 1–4.

Biäsing, J. & Krost, A. (2004). *Physica Status Solidi (A) Applied Research*, **201**(4), 17–20.

Chang, S.-L. (1982). *Journal of Applied Physics*, **53**(4), 2988.

Chuan-zheng, Y., Jian-min, H. a. O. & Guang-wen, P. E. I. (2000). *The Rigaku Journal*, **17**(1), 46–57.

Cole, H., Chambers, F. H. & Dunn, H. M. (1962). *Acta Crystallographica*, **15**(2), 138–144.

Cullity, B. D. & Stock, S. (2001). In *Elements of X-Ray diffraction*. USA: Addison-Wesley.

Domagała, J. Z., Morelhão, S. L., Sarzyński, M., Maździarz, M., Dłużewski, P. & Leszczyński, M. (2016). *Journal of Applied Crystallography*, **49**(June), 798–805.

Grundmann, M., Scheibe, M., Lorenz, M., Bläsing, J. & Krost, A. (2014). *Physica Status Solidi (B) Basic Research*, **251**(4), 850–863.

Grundmann, M. & Zúñiga-Pérez, J. (2015). *Physica Status Solidi (B)*, **253**(2), 351–360.

Hom, T., Kiszenik, W. & Post, B. (1975). *Journal of Applied Crystallography*, **8**(4), 457–458.

Isherwood, B. J., Brown, B. R. & Halliwell, M. A. G. (1981). *Journal of Crystal Growth*, **54**(3), 449–460.

Martínez-Tomás, M. C., Hortelano, V., Jiménez, J., Wang, B. & Muñoz-Sanjosé, V. (2013*a*). *CrystEngComm*, **15**(19), 3951.

Martínez-Tomás, M. C., Montenegro, D. N., Agouram, S., Sallet, V. & Muñoz-Sanjosé, V. (2013*b*). *Thin Solid Films*, **541**, 107–112.

Martínez-Tomás, M. C., Montenegro, D. N., Sallet, V. & Muñoz-Sanjosé, V. (2012). *Journal of Applied Physics*, **112**(1), 014305.

Morelhão, S. L. & Cardoso, L. P. (1991). *Journal of Crystal Growth*, **110**(3), 543–552.

Morelhão, S. L. & Cardoso, L. P. (1993). *Journal of Applied Physics*, **73**(9), 4218–4226.

Morelhão, S. L. & Cardoso, L. P. (1996). *Journal of Applied Crystallography*, **29**(4), 446–456.

Morelhão, S. L., Cardoso, L. P., Sasaki, J. M. & De Carvalho, M. M. G. (1991). *Journal of Applied Physics*, **70**(5), 2589–2593.

Morelhão, S. L. & Domagala, J. Z. (2007). *Journal of Applied Crystallography*, **40**(3), 546–551.

Morelhão, S. L., Quivy, A. A. & Härtwig, J. (2003). *Microelectronics Journal*, **34**(5-8), 695–699.

Ohtomo, A., Kawasaki, M., Koida, T., Masubuchi, K., Koinuma, H., Sakurai, Y., Yoshida, Y., Yasuda, T. & Segawa, Y. (1998). *Applied Physics Letters*, **72**(19), 2466–2468.

Post, B. (1975). *J. Appl. Cryst*, **8**, 452–456.

de Prado, E., Martínez-Tomás, M. C., Deparis, C., Muñoz-Sanjosé, V. & Zúñiga-Pérez, J. (Unpublised). *Unpublished*.

Renninger, M. (1937). *Zeitschrift für Physik*, **106**(November), 141–76.

Renninger, M. (1955). *Acta Crystallographica*, **8**(10), 606–610.

von Wenckstern, H., Schmidt-Grund, R., Bundesmann, C., Müller, A., Dietrich, C. P., Stölzel, M., Lange, M. & Grundmann, M. (2012). In *Handbook of Zinc Oxide and Related Materials*, vol. 1, chap. 10, pp. 257–320. Florida, USA: Francis/CR.

Zúñiga-Pérez, J., Consonni, V., Lymperakis, L., Kong, X., Trampert, A., Fernández, S., Brandt, O., Renevier, H., Keller, S., Hestroffer, K., Wagner, M. R., Sebastián, J., Akyol, F., Rajan, S., Rennesson, S., Palacios, T., Feuillet, G., Brandt, O., Renevier, H., Trampert, A., Fern, S., Keller, S., Hestroffer, K., Wagner, M. R. & Sebasti, J. (2016). *Applied Physics Reviews*, **3**(25), 041303.

Table 1. *Description of the samples*

Sample	% Mg (EDX)	Thickness ZnO buffer layer (nm)	Thickness $Zn_{1-x}Mg_xO$ layer (nm)
S27	27	45	525
S35	35	45	76
S43	43	45	188

Table 2. *Sets of planes that contribute to each hybrid peak and their corresponding peak positions. Full Width at Half Maximum is shown in brackets. All the angles are given in degrees.*

Peak	Reflections $\vec{S}+\vec{C}$	$Zn_{0.73}Mg_{0.27}O$ $2\theta_{exp}$ (FWHM)	$2\theta_{theo}$	φ_{exp} (FWHM)	φ_{theo}	$Zn_{0.65}Mg_{0.35}O$ $2\theta_{exp}$	$2\theta_{theo}$	φ_{exp}	φ_{theo}	$Zn_{0.57}Mg_{0.43}O$ $2\theta_{exp}$ (FWHM)	$2\theta_{theo}$	φ_{exp} (FWHM)	φ_{theo}
1	$(\bar{1}1.5)_S+(10.\bar{3})_L$		47.011	0.05	0.04		46.735	0.02	−0.27		46.522	−0.29	−0.44
	$(10.5)_S+(\bar{1}1.\bar{3})_L$		47.011	(1.11)	−0.04		46.735		0.27		46.523	(1.29)	0.44
2	$(0\bar{1}.3)_S+(02.\bar{1})_L$		47.020	61.36	62.02		46.692		62.01		46.531	59.88	62.00
	$(10.5)_S+(\bar{1}1.\bar{3})_L$		47.011	(1.06)	61.11		46.735	60.97	60.80		46.523	(1.01)	60.63
	$(00.4)_S+(01.\bar{2})_L$		47.061		61.34		46.797		61.19		46.613		61.12
3	$(02.\bar{1})_L+(0\bar{1}.3)_S$	47.005	47.020	119.10	117.94	46.80	46.692		118.02	46.486	46.531	118.83	118.00
	$(10\bar{3})_L+(\bar{1}1.5)_S$	(0.052)	47.011	(0.99)	118.88		46.735	120.34	119.35	(0.052)	46.522	(0.88)	119.48
	$(01.\bar{2})_L+(00.4)_S$		47.061		118.59		46.797		118.83		46.613		118.84
4	$(10.\bar{3})_L+(\bar{1}1.5)_S$		47.011	179.89	180.03		46.735	180.24	179.91		46.522	179.67	179.66
	$(\bar{1}1.\bar{3})_L+(10.5)_S$		47.011	(1.06)	−180.23		46.735		−179.91		46.523	(1.13)	−179.86
5	$(0\bar{1}.3)_S+(02.\bar{1})_L$		47.020	−61.12	−62.02		46.692		−62.01		46.531	−61.17	−62.00
	$(\bar{1}1.5)_S+(10.\bar{3})_L$		47.011	(0.86)	−61.11		46.735	-60.05	−60.80		46.523	(0.95)	−60.63
	$(00.4)_S+(01.\bar{2})_L$		47.061		−61.34		46.797		−61.19		46.613		−61.12
6	$(02.\bar{1})_L+(0\bar{1}.3)_S$		47.020	−119.10	−118.14		46.692		−118.02		46.531	−120.04	−118.20
	$(\bar{1}1.\bar{3})_L+(10.5)_S$		47.011	(1.11)	−119.08		46.735	-119.36	−118.83		46.522	(1.36)	−119.68
	$(01.\bar{2})_L+(00.4)_S$		47.061		−118.79		46.797		−118.83		46.613		−119.04
7	$(01.0)_L+(00.2)_S$		47.352	90.30	90.05		47.221	90.00	89.83		47.175	89.21	90.16
	$(00.2)_S+(01.0)_L$	47.350	47.352	(0.99)	89.90	47.24	47.221		90.18	47.172	47.175	(1.30)	89.8
8	$(01.0)_L+(00.2)_S$	(0.045)	47.352	−89.97	−90.25		47.221	−90.00	−90.18	(0.048)	47.175	−90.61	−90.36
	$(00.2)_S+(01.0)_L$		47.352	(0.98)	−89.90		47.221		−89.83		47.175	(1.30)	−89.80

Table 3. *Azimuthal deviations for the set of planes.*

Planes $\vec{S}+\vec{C}$	Beam path	$Zn_{0.73}Mg_{0.27}O$ $\Delta\varphi_{exp}$	$\Delta\varphi_{theo}$	$Zn_{0.57}Mg_{0.43}O$ $\Delta\varphi_{exp}$	$\Delta\varphi_{theo}$
$(\bar{1}1.5)_S+(10.\bar{3})_L$	0°/180°	0.16°	0.07°	0.04°	0.04°
$(10.5)_S+(\bar{1}1.\bar{3})_L$			0.27°		0.36°
$(0\bar{1}.3)_S+(02.\bar{1})_L$			0.17°		0.26°
$(10.5)_S+(\bar{1}1.\bar{3})_L$	60°/ − 120°	0.46°	0.20°	0.08°	0.37°
$(00.4)_S+(01.\bar{2})_L$			0.13°		0.22°
$(0\bar{1}.3)_S+(02.\bar{1})_L$			0.03°		0.06°
$(\bar{1}1.5)_S+(10\bar{3})_L$	−60°/120°	0.22°	0.00°	0.00°	0.05°
$(00.4)_S+(01.\bar{2})_L$			0.07°		0.10°
$(00.2)_S+(01.0)_L$	90°/ − 90°	0.27°	0.05°	0.18°	0.22°
$(01.0)_L+(00.2)_S$			0.15°		0.10°

Table 4. *Calculated lattice parameters of samples (±0.00007 nm)*

Experimental method	$Zn_{0.73}Mg_{0.27}O$ a (nm)	c (nm)	$Zn_{0.57}Mg_{0.43}O$ a (nm)	c (nm)
RSM of (01.2) and (01.4) reflections	0.32580	0.51757	0.32683	0.51445
HMD of (01.2) reflection	0.32582	0.51731	0.32676	0.51446

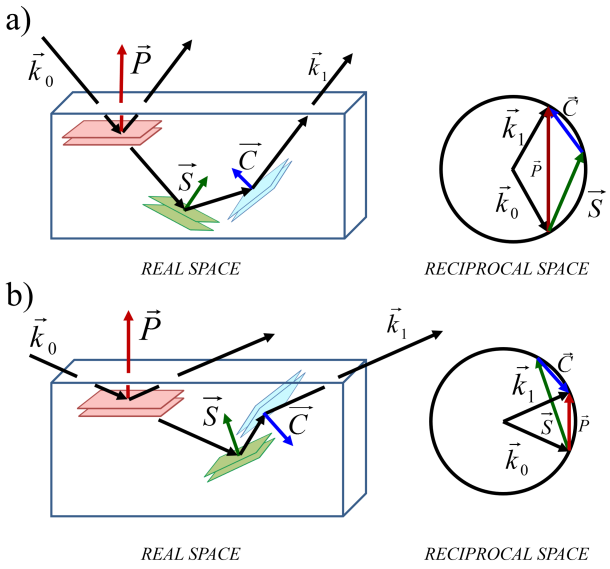

Fig. 1. Geometry of a three-beam MD in real and reciprocal space. The sum of secondary ($\vec{S}$) and cooperative ($\vec{C}$) vectors produces the primary one ($\vec{P}$). The incidence can take place a) at the upper side of both planes or b) at the upper/bottom side.

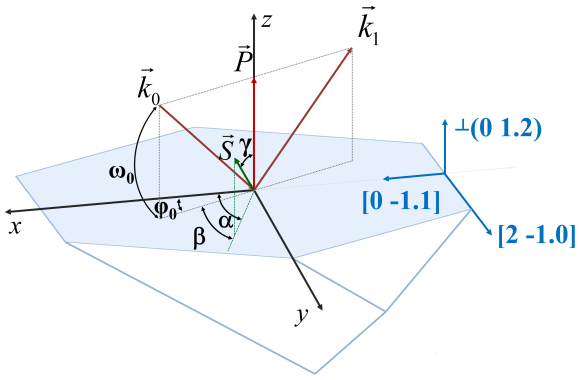

Fig. 2. Description of the angles and the selected orthogonal system employed for the theoretical calculation of HMD peaks.

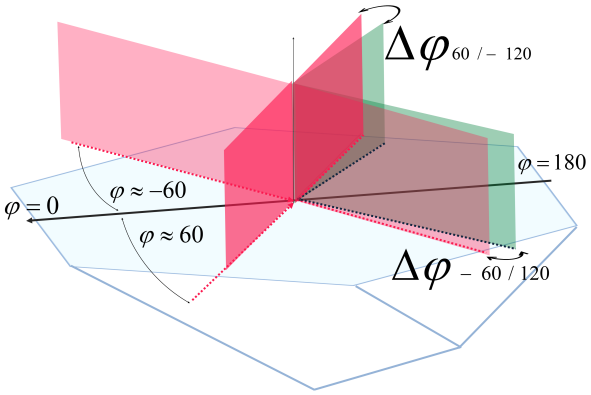

Fig. 4. Scheme of the different paths in the $60°/-120°$ and $-60°/120°$ trajectories.

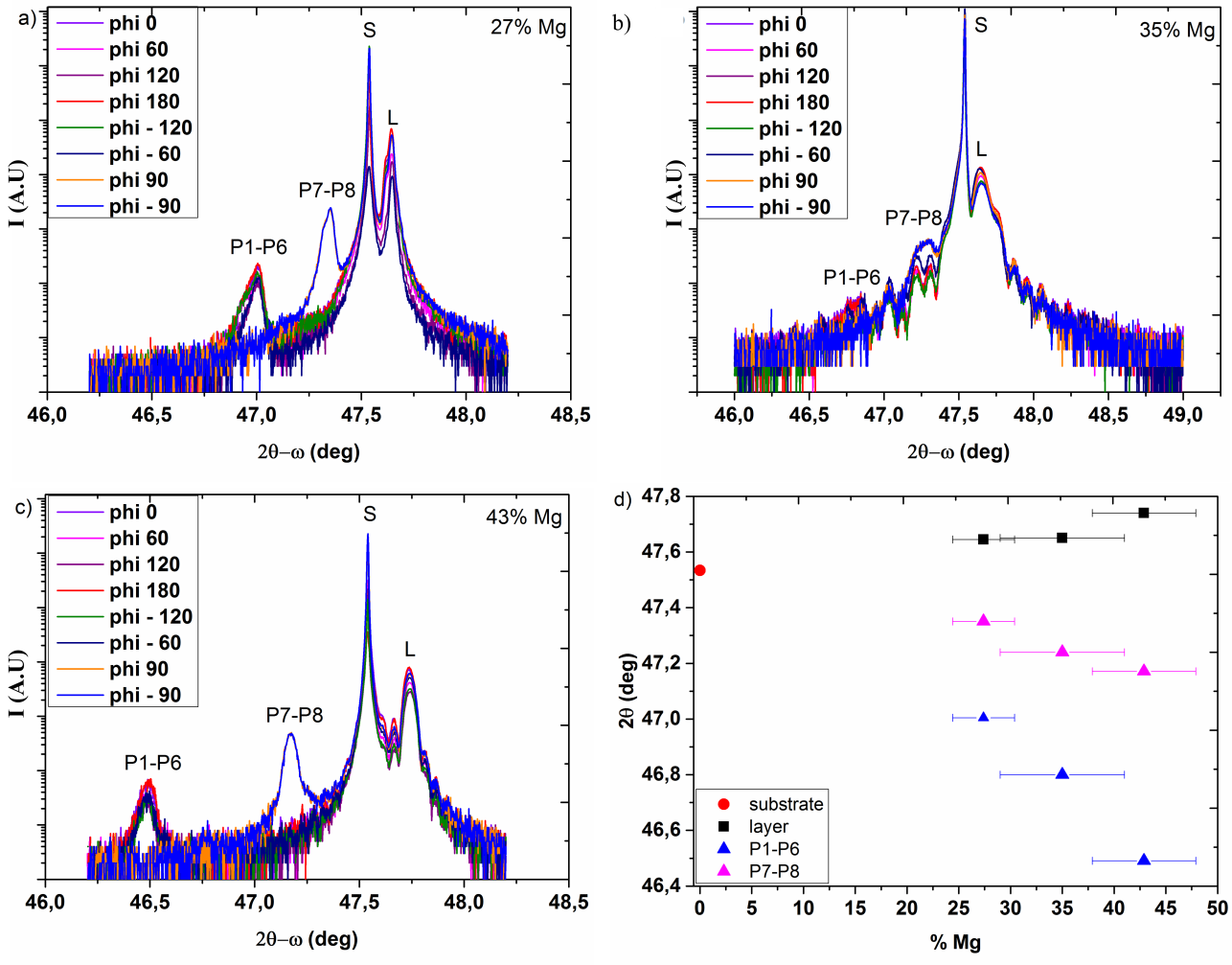

Fig. 5. $2\theta - \omega$ scans around (01.2) primary ZnO reflection for a) S27, b) S35 c) S43 samples; S/L indicates substrate or layer respectively. d) Bragg angle positions for the set of samples. P1-P6 correspond to hybrid reflections with six-fold symmetry and P7-P8 for such with two-fold symmetry.

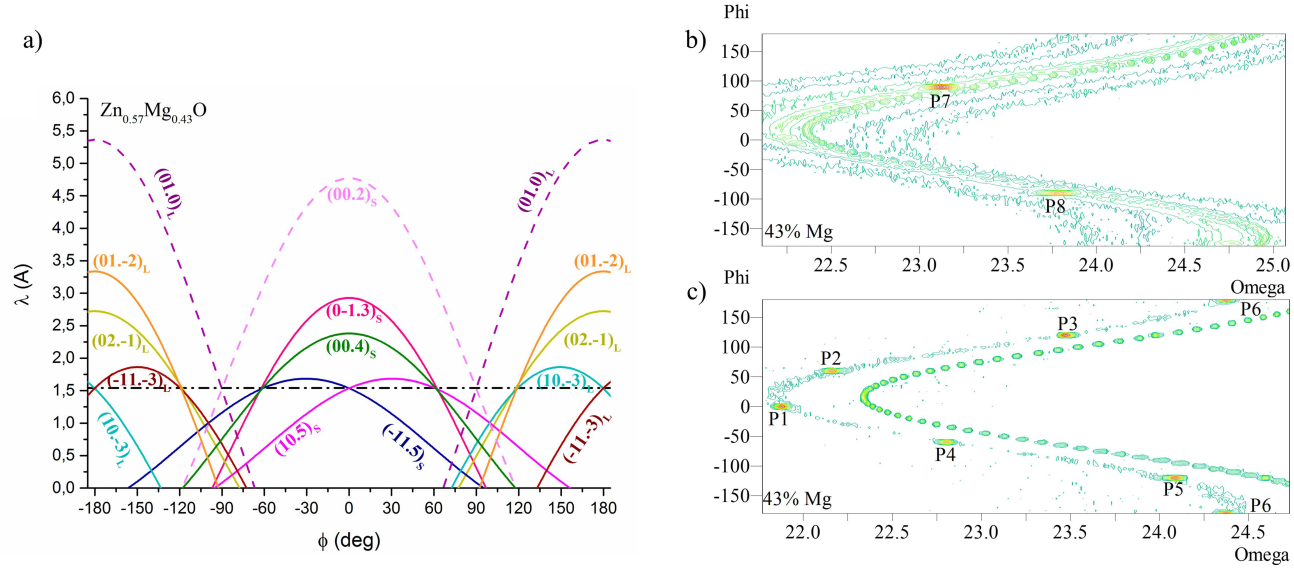

Fig. 6. a) Azimuthal positions at which HMD appears in sample S43 as a function of the wavelength for the considered set of planes. Solid/dashed line correspond to planes with 6-fold/2-fold symmetry respectively, b) c) phi/ω maps for hybrid peaks at both low and high Brag angles respectively.

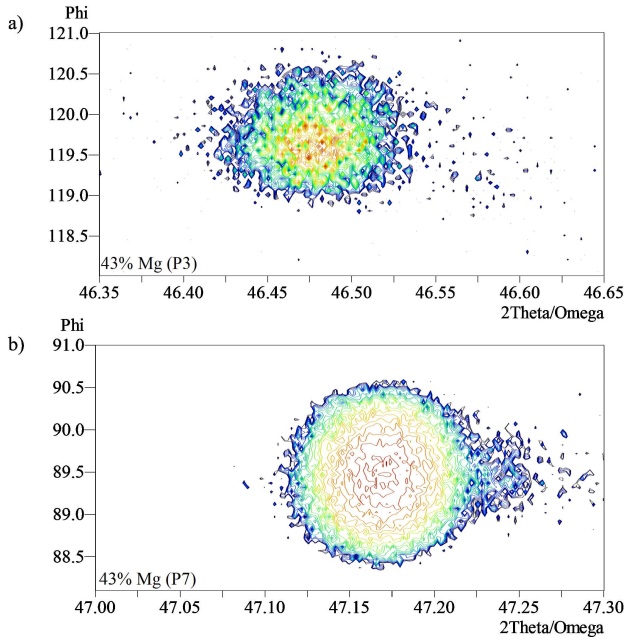

Fig. 7. *Phi*/$2\theta - \omega$ maps for sample S43 of peak a) P3 being the maximum intensity 7cps and b) P7 being the maximum intensity 72cps.

Synopsis

In this work, hybrid multiple diffraction has been employed to analyze r-oriented $Zn_{1-x}Mg_xO/ZnO$ systems. All the observed hybrid reflections have been explained, as well as indexed the planes that contribute and calculated the angles at which hybrid peaks are observed. In addition, the layer lattice parameters have been accurately determined by using the hybrid reciprocal space through one single measurement in standard symmetric conditions.